Optical excitation of multiple standing spin modes in three-dimensional optomagnonic nanocavities

Daria O. Ignatyeva[1,2,*] Denis M. Krichevsky[1,3,†] Dolendra Karki[4] Anton Kolosvetov[1,5]
Polina E. Zimnyakova[1] Alexander N. Shaposhnikov[6] Vladimir N. Berzhansky[6] Miguel Levy[4]
Alexander I. Chernov[1,5] and Vladimir I. Belotelov[1,2]

[1]*Russian Quantum Center, Moscow 121205, Russia*

[2]*Faculty of Physics, M.V. Lomonosov Moscow State University, Moscow 119991, Russia*

[3]*Moscow Institute of Physics and Technology (National Research University), Dolgoprudny 141700, Russia*

[4]*Physics Department, Michigan Technological University, Houghton, Michigan, USA*

[5]*Center for Photonics and 2D Materials, Moscow Institute of Physics and Technology (National Research University), Dolgoprudny 141700, Russia*

[6]*Institute of Physics and Technology, V.I. Vernadsky Crimean Federal University, Simferopol 295007, Crimea*

We report the experimental observation of multiple standing spin modes in a three-dimensional (3D) optomagnonic nanocavity formed by a nanometer-sized iron-garnet nanocylinder. We show that launching of the standing spin modes is achieved due to a high confinement of the optically generated effective magnetic field caused by the localized optical resonance. Quantization and spin-wave mode inhomogeneity are achieved in each of the three spatial dimensions. The presented approach opens horizons for 3D optomagnonics by combining nanophotonic and magnonic functionalities within a single nanocavity.

I. INTRODUCTION

Optomagnetism [1–3] is important for ultrafast, local, and reconfigurable spin control. This opens opportunities for fast and energy-efficient information processing [4,5], including quantum information technologies [6,7], logical elements [8,9], memory [10–14], dynamic holography [15], and other spin-based devices [16]. Optomagnetism is based on the action of the femtosecond laser pulse on the spin system of a magnetic material, which may lead to different scenarios of spin dynamics, including the excitation of spin precession and spin waves [17–22] and magnetization reversal [11,13,14,23].

Miniaturization is one of the key problems in optomagnetism due to a diffraction limit. To overcome this limit and excite spin dynamics at the nanoscale, various nanoplasmonic [24–29] and dielectric magnetophotonic [30–35] structures may be used to localize light at the spots of subwavelength dimensions. At the same time, the limited size of the optomagnetic cavity imposes selection rules on the spin wavevector and results in its quantization and the appearance of a set of standing spin modes. While for micrometer-sized objects the magnetostatic splitting of

such modes' eigenfrequencies is small [36], the situation drastically changes with the further miniaturization of the device size down to the nanometer scale. The considerable splitting of the frequencies of different spatial eigenmodes arises, in this case, due to the interplay of the magnetodipole and exchange interactions [32,34]. As a result, magnets smaller than a micron can be thought of as optomagnonic nanocavities supporting both localized optical and spin modes.

The optical impact on spins can be described in terms of an effective magnetic field induced by light inside a magnet [2]. Localization and the direction of the optically induced effective magnetic field can be easily tuned in the nanostructure by varying the parameters of the laser pulse. It allows one to selectively excite the desired modes [32,34]. This is an important advantage of the optomagnetic means compared to the traditional ones using the ferromagnetic resonance technique and microwave antennas [37–39]. Apart from that, addressing a single nanomagnet via a microscopic nanoantenna requires its precise positioning, for example, via the movable substrate [40], increasing the complexity of the setup and likely limiting the operation rate.

Recently demonstrated high-order spin modes excited optomagnetically by laser pulses in smooth films [41,42] and nanophotonic structures [32,34] are standing spin

---

*daria.ignatyeva@gmail.com

†krichevskii.dm@phystech.edu

waves across the film thickness, while in the lateral direction they still possess quasihomogeneous profiles.

Here, we take the next step forward and report optical excitation of standing spin modes in optomagnonic nanocavities confined in all three spatial dimensions. We demonstrate that a femtosecond laser pulse in a magnetic nanocylinder acts like a pointlike source of magnetization dynamics due to the excited localized optical modes of the nanocylinder providing a highly confined effective magnetic field. Due to this, a set of nanocavity spin modes of different orders with different frequencies is launched.

II. METHODS

A. Sample fabrication

First, bismuth-substituted iron-garnet $Bi_{1.0}Lu_{0.5}Gd_{1.5}$ $Fe_{4.2}Al_{0.8}O_{12}$ (BIG) film of 515 nm thick was deposited via magnetron sputtering on a SiO_2 substrate. The nanocylinder arrays were then fabricated via *e*-beam lithography and argon-ion-beam sputter etching. The nanocylinder patterns were written on 550-nm-thick positive *e*-beam resist (ZEP-520A) by 100-keV *e*-beams (VISTEC EBPG 5000+) exposed to a uniform dose of 140 $\mu C/cm^2$ after proximity-effect correction. Since ZEP is a nonconducting polymer resist, a 30-nm-thick conducting gold-layer coating was sputter deposited on top and grounded via conducting copper tape to avoid distortions of the *e*-beam due to electrical charging during the *e*-beam writing procedure. The exposed resist was developed in an amyl acetate solution after the removal of the gold layer in gold etchant solution first. The nanocylinder resist patterns were then printed onto the BIG film by slow sputter etching at a rate of 2.5 nm/min in an argon-ion mill system (Intlvac Nanoquest; beam parameters: beam voltage, 200 V; accelerating voltage, -24 V; beam current, -70 mA; and plasma forward power, 71 W). The sample stage was cooled to 6°C throughout etching to prevent hardening of the resist. Finally, the remaining thin layer of the resist was removed by using resist remover, *N*-methyl-2-pyrrolidine solution, heated at 80°C.

B. Time-resolved optomagnetic measurements

Spin dynamics in the sample was experimentally measured using a time-resolved magneto-optical pump-probe scheme. Pump and probe pulses were generated by an Avesta TOPOL parametric oscillator pumped by a Yb-doped Avesta TEMA laser [(80 ± 5)-MHz repetition rate, 180-fs pulse duration]. Pump pulses of 730-nm wavelength were utilized to excite the system, and linearly polarized probe pulses of 525 nm were used to detect spin dynamics via the Faraday effect. Delayed pump pulses were modulated using a photoelastic modulator (Hinds Instruments PEM 100). The polarization changes of the probe pulse passed through the sample due to the Faraday effects were
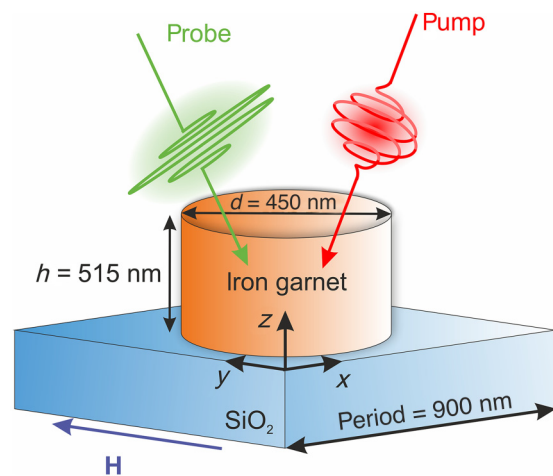

FIG. 1. Configuration of magneto-optical pump-probe experiments. Unit cell of the nanostructure under in-plane external magnetic field is excited by circularly polarized pump pulse and probed by linearly polarized light.

measured using an autobalanced optical receiver (Nirvana 2007) in a lock-in detection scheme. The sample was placed in the in-plane field of an electromagnet. The scheme of the measurement configuration is presented in Fig. 1.

C. Optical simulations

Electromagnetic simulations of optical modes inside the unit cell of the considered all-dielectric nanostructure were carried out by numerical solution of Maxwell equations using the rigorous coupled-wave analysis approach [43,44]. Bloch boundary conditions were applied to the unit cell to simulate an infinite array (along the *x* and *y* axes, see Fig. 1). A plane-wave excitation was utilized. The dispersion of BIG dielectric permittivity was taken into account [45]. Permittivity spectra of BIG for the 550–1000-nm spectral region are presented in Fig. 2. The refractive index of SiO_2 was equal to 1.45.

D. Micromagnetic simulations

We built a numerical model of a bismuth-substituted iron-garnet nanocavity using the micromagnetic platform mumax3 [46]. Micromagnetic modeling was first performed for a smooth 515-nm-thick film to verify the material parameters, such as saturation magnetization, $M_s = 160$ kA/m; anisotropy constant, $K_u = 2000$ J/m^3; and exchange stiffness, $A_{ex} = 7.5 \times 10^{-12}$ J/m. The resonant frequencies of magnetization precession obtained for the different values of the external field show good agreement with the experimental results (Fig. 3).

In a real experiment, a femtosecond laser pulse creates a short effective magnetic field via the inverse Faraday effect. This field acts like a knock, launching several spin
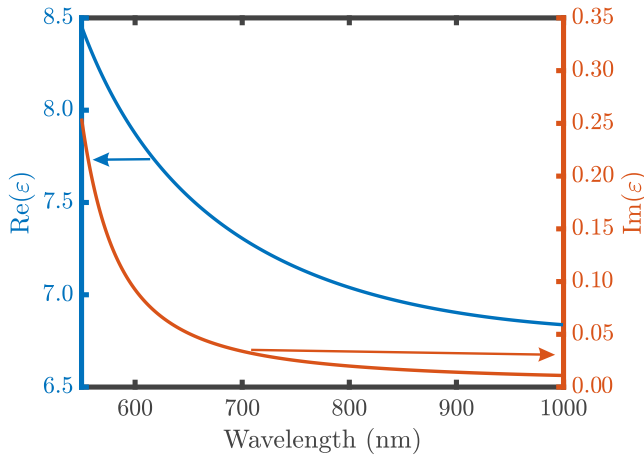
FIG. 2. Dielectric permittivity spectra of BIG.

modes of the magnetic system. The analysis of these spin modes was performed by the following method of finding the eigenfrequencies and modes of the magnetic cavity.

First, the $H_{\text{exc}}(t) \propto \sin(2\pi f_0 t)/(2\pi f_0 t)$ excitation magnetic field pulse with a broadband spectrum was applied to the central part of the nanocylinder. Fourier analysis of the time-dependent magnetization component, $m_z(t)$, revealed several peaks corresponding to the resonant spin-mode frequencies, f_j. To study the profiles of the modes with these f_j resonance frequencies, a harmonic time-varying excitation magnetic field, $H_{\text{exc}} \propto \sin(2\pi f_j t)$, was applied to the central area of a nanocavity. After $N \sim 15 \gg 1$ periods of the excitation magnetic field, the spin dynamics reached the stationary regime with $m_z(x, y, z)$ distribution, corresponding to the mode at this frequency. This is a standard technique in mumax3 (see Ref. [47]) that allows for eigenmode analysis. As the spatial distribution of H_{exc} coincides with the calculated H_{IFE}, a comparison of frequencies obtained in experiments and simulations allows us to identify the modes that are excited by a laser pulse.
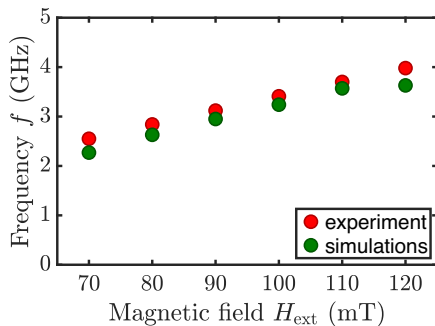

FIG. 3. Resonant frequencies of magnetization precession in a smooth film obtained for different values of external magnetic field experimentally and numerically. Composition and thickness of iron garnet are the same as those used for nanocavity fabrication.

III. RESULTS AND DISCUSSION

Optical excitation of the confined spin waves is performed by illuminating an array of bismuth-substituted iron-garnet nanocylinders with femtosecond laser pulses. The nanocylinders are 450 nm in diameter and 515 nm in height. They are periodically arranged in a two-dimensional square lattice with a period of $P = 900$ nm (see Sec. II for fabrication details). The large separation between the cylinders makes both optical [48] and magnetodipole interactions between them negligible. Thus, both the optical and spin-mode properties of the system are mostly determined by the properties of an individual nanocylinder.

The transmittance spectrum [Fig. 4(a)] of a nanocylinder exhibits a set of optical resonances excited in a dielectric nanocylinder. These resonances may be described as the Fabry-Perot resonances of the guided modes of the cylindrical waveguides [48]. The electromagnetic field of light is strongly localized inside the nanocylinder. Consequently, circular polarization of the incident pulse induces the effective magnetic field via the inverse Faraday effect [2] (IFE) $\mathbf{H}_{\text{IFE}} \propto \text{Im} [\mathbf{E} \times \mathbf{E}^*]$ directed predominantly along the z axis, which is also localized within the nanocylinder, as shown in the insets of Fig. 4(a) and in Fig. 4(b).

For optical excitation of the spin modes, we choose the resonance at a wavelength of $\lambda = 730$ nm. This wavelength is in the optimal spectral range for the magneto-optical figure of merit, which is due to a sort of trade-off between the high gyration values and the low damping of the iron-garnet material itself. It allows one to perform optical pumping quite efficiently and to avoid thermal effects. Since at this wavelength iron garnets are rather transparent, the main impact of circularly polarized pulses on spins is due to the inverse Faraday effect [2].

Figure 4(b) shows a strong confinement of the effective magnetic field, H_{IFE}, induced by a laser pulse via the IFE in the central part of a cylinder. While the volume of the nanocylinder itself is $V_{\text{cyl}} = 8 \times 10^{-2}$ μm³, the effective volume of the laser-induced IFE field, calculated as $V_{\text{IFE}} = \int H_{\text{IFE}}(\mathbf{r}) dV / \max |H_{\text{IFE}}|$, is an order lower, $V_{\text{IFE}} = 7.6 \times 10^{-3}$ μm³. This causes the optical pump to act as a pointlike source, exciting multiple standing spin modes.

A similar situation is observed at other wavelengths. For example, the transmittance maxima at about 800 nm [Fig. 4(a)] are also caused by interference inside a nanocylinder. The effective volume of the laser-induced IFE field is $V_{\text{IFE}} = 3.0 \times 10^{-3}$ μm³. At the same time, the distribution of the IFE field is quite different. Remarkably, one of the field antinodes is located at the cylinder surface.

Nanocylinders were magnetized up to saturation by an in-plane magnetic field, $\mathbf{H}_{\text{ext}}$, applied to the sample in plane, perpendicular to the axes of the cylinders. It is
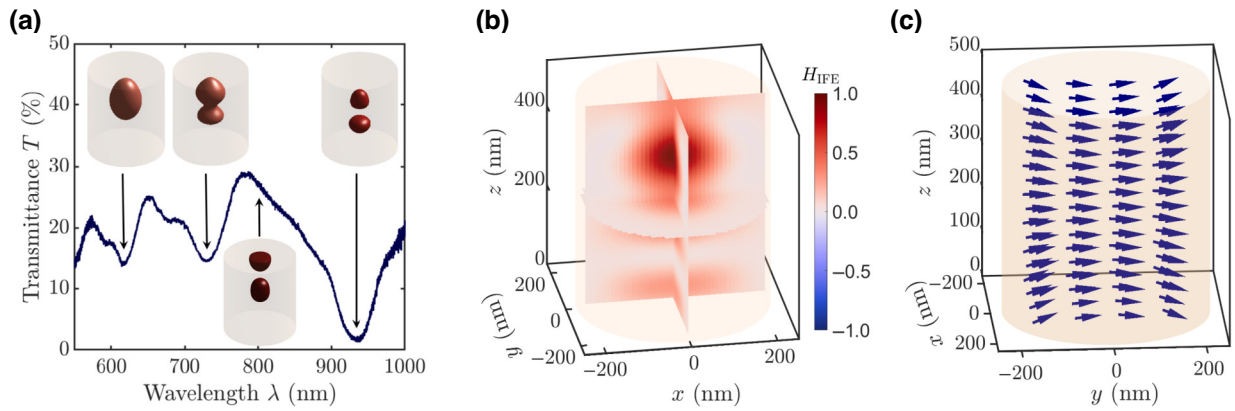
FIG. 4.   Optical excitation of spin modes. (a) Experimental transmittance spectra of the nanocylinder array. Insets represent regions inside the nanocylinder where the z component of the H_{IFE} field is maximal, shown as the isosurfaces at the e^{-1} level. (b) Distribution of the H_{IFE} field's z component (normalized to its maxima) inside a nanocylinder calculated at $\lambda = 730$-nm wavelength shown at three central cross sections of a cylinder. (c) Nanocylinder static magnetization under external magnetic field, $H_{\text{ext}} = H_y$, applied perpendicular to its axis.

important that the height, h, and diameter, d, of the cylinder are similar to each other, $h \approx d$, so that the aspect ratio of the nanocavity is close to 1:1. This makes the contribution of the demagnetizing fields quite prominent. The resulting magnetization direction inside the cylinder is inhomogeneous [Fig. 4(c)]. A significant tilt of the static magnetization from the $\mathbf{H}_{\text{ext}}$ direction, an increase of the normal, and a decrease of the in-plane magnetization components emerge near the cylinder walls. Such a peculiar magnetization distribution makes the frequencies of the modes sensitive to their localization and amplitude distribution inside the nanocavity. The difference in spin-mode frequencies excited in a nanocavity is important, since it allows us to identify and study the modes separately.

The effective magnetic field generated by the femtosecond laser pulse via the IFE deflects the magnetization from its equilibrium value, and thus, launches the spin dynamics. The high confinement of this field makes optical excitation similar to a pointlike source, and thus, makes it possible to excite a set of standing spin modes with inhomogeneous and sign-changing profiles. The frequencies of these modes are different from each other for the following reasons. First of all, according to the numerical simulations of demagnetizing fields (see Sec. II for micromagnetic simulation details), the magnetization of the cylinder is nonuniform, and in-plane components decrease near the cylinder walls [Fig. 4(c)]. Thus, the frequencies of the modes localized near the cylinder walls would be smaller than the ones localized at the cylinder center. Apart from that, the more inhomogeneous a mode profile is, the more significant the exchange-field contribution is, and the higher the spin-mode frequency is.

Simultaneous excitation of multiple spin modes results in a complex beating pattern of the temporal dependence of the magnetization precession itself [Fig. 5(a)]. The

Fourier spectra show several distinct peaks corresponding to the eigenfrequencies of the excited modes [Fig. 5(b)]. A detailed analysis of the excited-spin-mode profiles with the corresponding frequencies is provided below. Hereafter, we mark these peaks as (n_x, n_y, n_z), according to the nature of the standing spin modes and the corresponding number of nodes along the x, y, z spatial directions.

The eigenfrequencies of the spin modes depend on the external magnetic field, H_{ext}, applied to the nanocylinder. Experimental results [Fig. 5(c)] show a good qualitative correspondence with the numerical simulations [Fig. 5(d)], while some quantitative differences might be caused by inaccuracies in nanocylinder fabrication processes. The numerical simulations of spin dynamics were performed using mumax3 software [46] (see Sec. II for details). At the same time, the analytical description of the nanocylinder eigenmodes is quite complicated. On one hand, as the ratio of the height to the diameter of the nanocavity is nearly 1:1, there are 3 degrees of freedom. On the other hand, demagnetizing fields are significant, and the axial symmetry is broken by the external magnetic field, H_{ext}, applied perpendicular to the nanocylinder axis. Good agreement between the experimental results and numerical simulations makes it possible to perform a numerical analysis of the profiles and types of spin modes excited in a nanocavity.

Figure 6 shows the three-dimensional (3D) profiles and central cross sections of the m_z oscillating component of the standing spin modes launched in a nanocavity by a femtosecond laser pulse (see Fig. 5). One might see that all three standing spin modes excited in a nanocavity have quite complex profiles, and a sign change is observed in all three spatial directions. This confirms that spin dynamics in the 3D optomagnonic nanocavity really has 3 degrees of freedom. Let us discuss the nature of the excited standing spin modes in more detail by analyzing the mode profiles
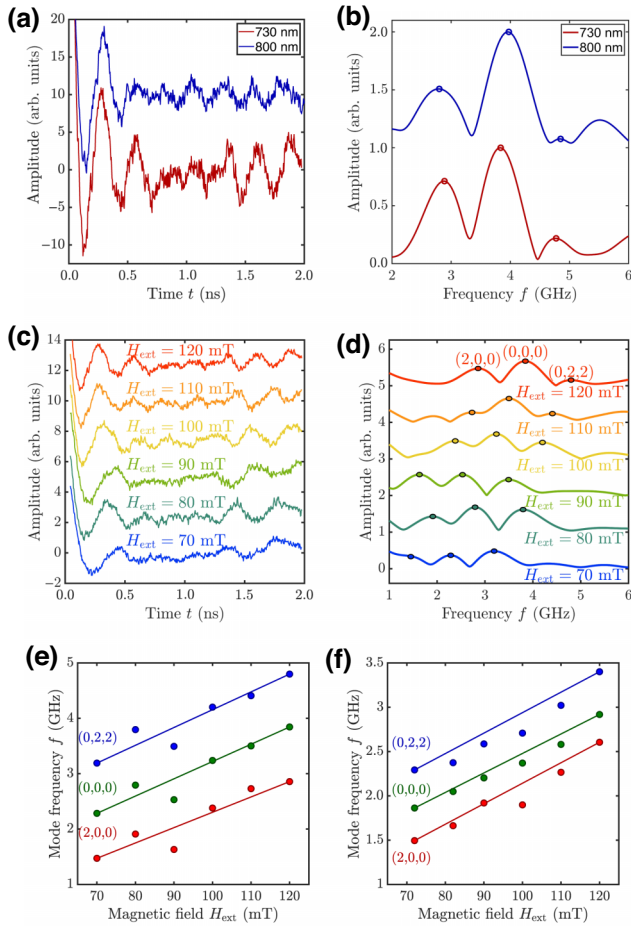
FIG. 5. Spin dynamics in the nanocylinder excited by a femtosecond pulse. (a) Magnetization precession and (b) its Fourier spectra measured for 120-mT external magnetic field by the transient Faraday rotation of the probe pulse for 730-nm (red curves) and 800-nm (blue curves) pump pulses. (c) Magnetization precession and (d) its Fourier spectra measured for different external magnetic fields by the transient Faraday rotation of the probe pulse for 730-nm pump pulses. Peaks corresponding to the excited standing spin modes are marked in (b),(d) as (n_x, n_y, n_z), according to the number of nodes along a certain direction (see details in the text). Magnetic field dependence of the frequencies of standing spin modes obtained (e) experimentally and (f) numerically.

and identifying the number of nodes, n_x, n_y, and n_z, in the corresponding spatial directions.

The amplitude of the standing spin mode with the lowest frequency [$(2, 0, 0)$] is high near the nanocavity edges. Such a mode is similar to the edge spin mode of a disk [49,50]; therefore, due to the demagnetization fields, it has a lower frequency than the other modes. At the same time, although the magnitude of m_z decreases in the central part, it obviously has two nodes along the x direction, while the phase in the y and z directions is quite homogeneous, so that it might be identified as the $n_x = 2, n_y = 0, n_z = 0$ edgelike standing spin mode.

The mode marked as $(0, 0, 0)$ is characterized by a quite homogeneous distribution of the m_z component inside a nanocavity. This makes it analogous to the fundamental mode of a nanocavity, except for some inhomogeneities at the nanocylinder edges. Therefore, this mode can be identified as the quasihomogeneous mode of a nanocavity.

The mode with the highest frequency observed in both experiments and simulations is characterized by two nodes in the y and z spatial directions, so that it might be identified as the $(0, 2, 2)$ standing spin mode. This is quite a remarkable result, since such a mode has a nearly zero average value of $\langle m_z \rangle = 1/V_{cyl} \int_{V_{cyl}} m_z(\mathbf{r}) d\mathbf{r}$. On the other hand, the spatial scale of the mode-profile inhomogeneity is about 150 nm. An ability to efficiently excite modes with such an amplitude distribution is due to a high localization of the optically generated effective magnetic field [Fig. 4(b)]. Actually, the distance between the two neighboring nodes of this mode is close to the H_{IFE} spot size inside a cylinder, which makes it the highest-order mode excited in this configuration.

The beating precession patterns with multiple peaks in their Fourier spectra are observed for two different wavelengths, i.e., 730 and 800 nm [Figs. 5(a) and 5(b)]. Both fundamental $(0, 0, 0)$ and edgelike $(2, 0, 0)$ modes are excited with quite high efficiency. However, the $(0, 2, 2)$ standing spin mode is almost absent from the spectra of the dynamics launched by a 800-nm laser pulse. This is due to IFE field localization both in the center and at the surface of a nanocylinder, which provides the same torque for these areas. At the same time, the sign change along the nanocylinder axis profile of this mode requires either a more localized spin-wave source or a sign-changing torque inside this volume. Thus, variation of the laser wavelength might lead to the tuning of the spin modes' excitation efficiency. This is an important point from a practical point of view. We report the experimental observation of the optomagnetic excitation of standing spin modes that are quantized and inhomogeneous in all three spatial dimensions of a nanocavity. Due to the submicron size and consequent contributions of the exchange interaction and demagnetizing fields to spin dynamics, the frequencies of these modes differ significantly. Moreover, one may control the spin modes' frequency splitting and magnitudes by the design of the nanocavity shape, for example, fabrication as nanocubes and nanoprisms. This opens wide opportunities for multichannel optomagnonic devices working simultaneously with several spin modes at different frequencies.

High confinement of the optically generated effective magnetic field makes it possible to excite standing spin modes with inhomogeneous and sign-changing profiles. Qualitatively, the amplitude, A, of the certain spin mode with $m_z(\mathbf{r})$ distribution launched by the excitation magnetic field, $H_{exc}(\mathbf{r})$, can be estimated as an overlap integral, $A \propto \int_V m_z(\mathbf{r}) H_{exc}(\mathbf{r}) dV$. Thus, if spin
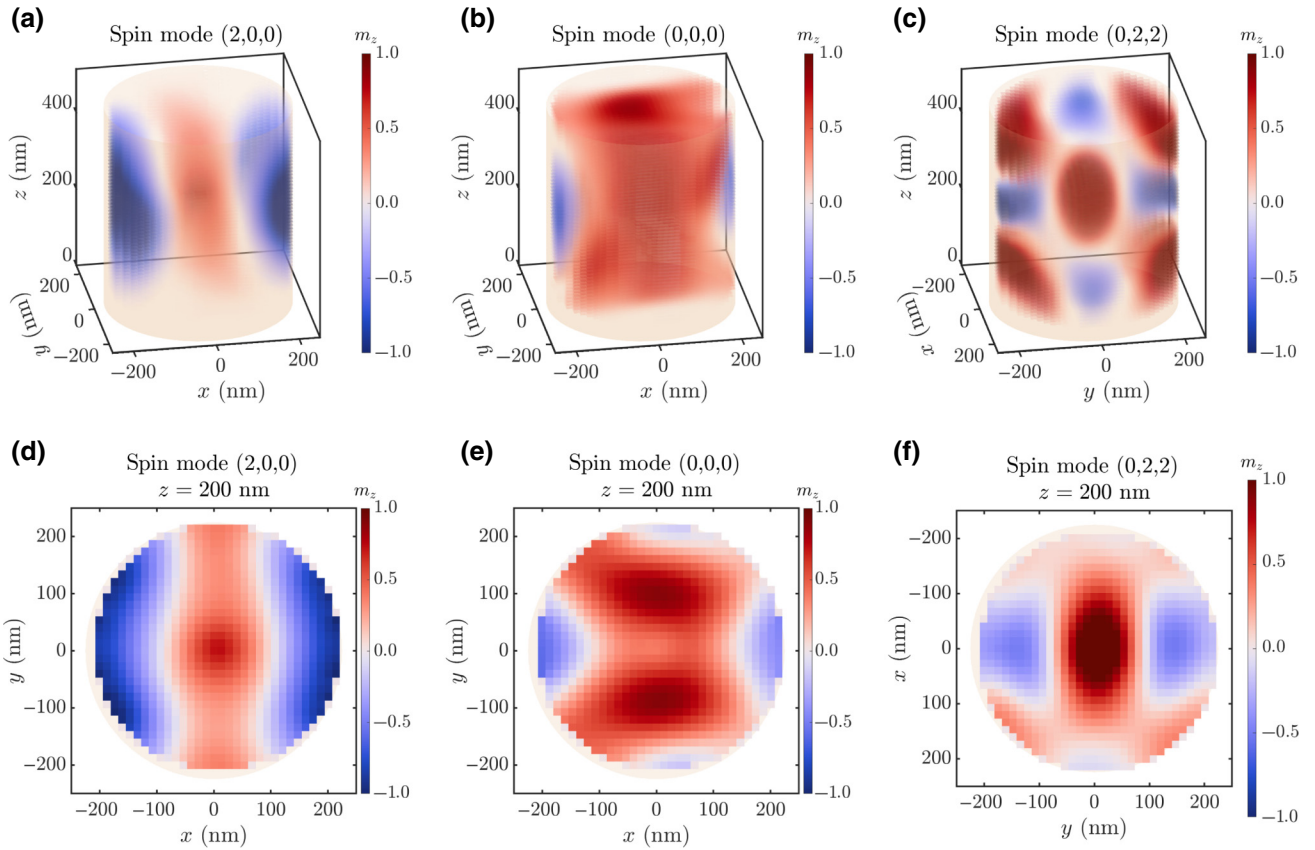
FIG. 6. Spin-mode 3D profiles (top panel) and central cross sections (bottom panel) of the m_z oscillating component of (a),(d) edge-like standing spin mode $(2, 0, 0)$; (b),(e) quasihomogeneous mode $(0, 0, 0)$; and (c),(f) standing spin mode $(0, 2, 2)$. Each distribution is normalized to m_z maximum of the corresponding spin mode. External magnetic field is 110 mT.

dynamics is launched by a quasihomogeneous optically induced or microwave magnetic field, $H_{\text{exc}}(\mathbf{r}) \approx \text{const}$, high-order modes with $n_j > 0$ characterized by $\langle m_z \rangle \sim 0$ are excited with small amplitudes (see Ref. [32], for example).

In the studied nanocavity, the magnitudes of the excited standing spin modes are nearly the same [Fig. 5(b)], although two of them, $(2, 0, 0)$ and $(0, 2, 2)$, are characterized by very inhomogeneous profiles. One can numerically characterize the homogeneity of the spin-mode profile with a value of $\eta = \langle m_z \rangle / \langle |m_z| \rangle$, with $\eta = 1$ for the homogeneous modes and $\eta \to 0$ with an increase of the inhomogeneity. In our case, $\eta = 0.9$ for quasihomogeneous mode $(0, 0, 0)$, and $\eta = 0.5$ and $\eta = 0.2$ for $(0, 2, 2)$ and $(2, 0, 0)$ modes, respectively. Excitation of such inhomogeneous standing spin modes is possible due to a high confinement of the optically generated inverse Faraday effect field.

Notably, the frequencies of the observed spin modes can be tuned by the design of the nanocavity shape. To illustrate this statement, we considered three types of shapes: cuboid, hexagonal, and triangular prisms. For each nanocavity, the height equals that of the nanocylinder

(515 nm). Each nanocavity has a differently shaped cross section, which is perpendicular to the nanocavity axis. Characteristic edge lengths for these shapes were chosen to provide similar cross-section areas. The characteristic length of the cross-section side equals 450 nm (cuboid → square cross section), 186 nm (hexagonal prism → hexagonal cross section), and 450 nm (triangular prism → triangle cross section). Spin-wave spectra for each of the proposed shapes excited by a source localized at the center contained three resonant peaks [Fig. 7(a)]. Figures 7(b)–7(d) show the peak positions as a function of external magnetic field. At low external fields (e.g., at 70 mT), the frequencies of the $(2,0,0)$ mode are separated by 0.5 GHz [Fig. 7(b)]. Notably, there is almost no separation between the mode frequencies for the cuboid and triangular prism. Similar behavior is observed for the $(0,0,0)$ and $(0,2,2)$ modes [Figs. 7(c) and 7(d)]. In the latter case, the frequency split does not exceed 0.25 GHz. The increase of the external magnetic field up to 120 mT makes the mode frequencies for the hexagonal prism and cylinder almost degenerate, while remaining separate for the cube and triangle. Consequently, the decrease in the number of sides of the cross section detunes the frequencies of the
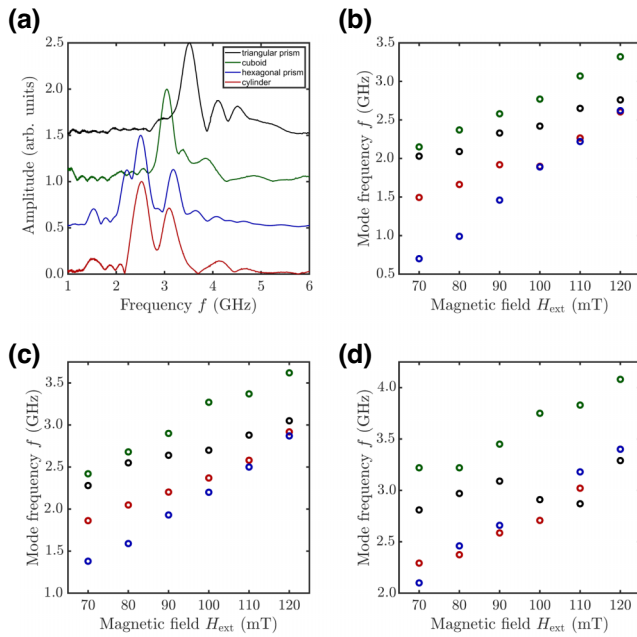
FIG. 7. Mode frequencies for different shapes of a nanoelement in comparison with the nanocylinder. Black represents a triangular prism, blue represents a hexagonal prism, green represents a cuboid, and red represents a cylinder. External magnetic field is 110 mT.

modes from the nanocylinder case. The frequency shift can exceed 1 GHz.

An optically localized resonance produces an effective magnetic field concentrated in the center of a nanocavity. At the same time, the utilization of nanophotonic structures [31] with other types of optical modes and other optomagnetic effects [2], such as the inverse Cotton-Mouton effect or the inverse transverse magneto-optical Kerr effect, might open wide possibilities for performing launching of the other orders of spin modes via different shapes and phase profiles of the exciting magnetic field. Moreover, nanophotonics provides a powerful means to easily tune the types of excitations by changing the characteristics of the femtosecond pulses, such as their polarization and wavelength, which allows us to switch between different optical modes in one nanocavity.

IV. CONCLUSION

We report an experimental observation of standing spin modes that are quantized and inhomogeneous in all three spatial dimensions. The recipe for their excitation involves femtosecond laser pulses illuminating an optomagnonic nanocavity at a wavelength of some optical resonance of the nanocavity. The optically induced field of the inverse Faraday effect is localized at the scale of a few hundred nanometers, thus providing a necessary pointlike instant

impact on spins and launching a set of different standing spin modes. Among them, the most interesting mode is the one with nodes in both lateral and longitudinal directions. Apart from that, its averaging along the whole nanocylinder is close to zero. Its excitation most vividly demonstrates the advantages of nanophotonics optomagnetism with respect to conventional means of spin-wave excitation. The presented approach opens opportunities for multichannel optomagnonic devices tunably launching several spin modes at different frequencies. The observed inhomogeneous distribution of spin modes is also promising for cavity optomagnonics [51], for which the coupling between optical modes and magnons was demonstrated recently [52].

[1] A. Kimel, A. Zvezdin, S. Sharma, S. Shallcross, N. De Sousa, A. García-Martín, G. Salvan, J. Hamrle, O. Stejskal, J. McCord, *et al.*, The 2022 magneto-optics roadmap, J. Phys. D: Appl. Phys. **55**, 463003 (2022).

[2] A. M. Kalashnikova, A. V. Kimel, and R. V. Pisarev, Ultrafast opto-magnetism, Physics-Uspekhi **58**, 969 (2015).

[3] A. V. Kimel, A. Kirilyuk, and T. Rasing, Femtosecond opto-magnetism: Ultrafast laser manipulation of magnetic materials, Laser Photon. Rev. **1**, 275 (2007).

[4] Y. Kajiwara, K. Harii, S. Takahashi, J.-i. Ohe, K. Uchida, M. Mizuguchi, H. Umezawa, H. Kawai, K. Ando, K. Takanashi, *et al.*, Transmission of electrical signals by spin-wave interconversion in a magnetic insulator, Nature **464**, 262 (2010).

[5] J. Chen, H. Wang, T. Hula, C. Liu, S. Liu, T. Liu, H. Jia, Q. Song, C. Guo, Y. Zhang, *et al.*, Reconfigurable spin-wave interferometer at the nanoscale, Nano Lett. **21**, 6237 (2021).

[6] J. Li, Y.-P. Wang, W.-J. Wu, S.-Y. Zhu, and J. You, Quantum network with magnonic and mechanical nodes, PRX Quantum **2**, 040344 (2021).

[7] D. Lachance-Quirion, Y. Tabuchi, A. Gloppe, K. Usami, and Y. Nakamura, Hybrid quantum systems based on magnonics, Appl. Phys. Express **12**, 070101 (2019).

[8] A. Kolosvetov, M. Kozhaev, I. Savochkin, V. Belotelov, and A. Chernov, Concept of the optomagnonic logic operation, Phys. Rev. Appl. **18**, 054038 (2022).

[9] M. Jamali, J. H. Kwon, S.-M. Seo, K.-J. Lee, and H. Yang, Spin wave nonreciprocity for logic device applications, Sci. Rep. **3**, 1 (2013).

[10] A. V. Kimel and M. Li, Writing magnetic memory with ultrashort light pulses, Nat. Rev. Mater. **4,** 189 (2019).

[11] C. D. Stanciu, F. Hansteen, A. V. Kimel, A. Kirilyuk, A. Tsukamoto, A. Itoh, and T. Rasing, All-optical magnetic recording with circularly polarized light, Phys. Rev. Lett. **99,** 047601 (2007).

[12] M. Gündoğan, P. M. Ledingham, K. Kutluer, M. Mazzera, and H. De Riedmatten, Solid state spin-wave quantum memory for time-bin qubits, Phys. Rev. Lett. **114,** 230501 (2015).

[13] A. Stupakiewicz, K. Szerenos, M. Davydova, K. Zvezdin, A. Zvezdin, A. Kirilyuk, and A. Kimel, Selection rules for all-optical magnetic recording in iron garnet, Nat. Commun. **10,** 612 (2019).

[14] A. Stupakiewicz, K. Szerenos, D. Afanasiev, A. Kirilyuk, and A. Kimel, Ultrafast nonthermal photo-magnetic recording in a transparent medium, Nature **542,** 71 (2017).

[15] M. Makowski, J. Bomba, A. Frej, M. Kolodziejczyk, M. Sypek, T. Shimobaba, T. Ito, A. Kirilyuk, and A. Stupakiewicz, Dynamic complex opto-magnetic holography, Nat. Commun. **13,** 7286 (2022).

[16] S. A. Nikitov, D. V. Kalyabin, I. V. Lisenkov, A. N. Slavin, Y. N. Barabanenkov, S. A. Osokin, A. V. Sadovnikov, E. N. Beginin, M. A. Morozova, Y. P. Sharaevsky, *et al.*, Magnonics: A new research area in spintronics and spin wave electronics, Physics-Uspekhi **58,** 1002 (2015).

[17] T. Satoh, Y. Terui, R. Moriya, B. A. Ivanov, K. Ando, E. Saitoh, T. Shimura, and K. Kuroda, Directional control of spin-wave emission by spatially shaped light, Nat. Photonics **6,** 662 (2012).

[18] M. R. Freeman and Z. Diao, All-optical spin-wave control, Nat. Photonics **6,** 643 (2012).

[19] I. Savochkin, M. Jäckl, V. Belotelov, I. Akimov, M. Kozhaev, D. Sylgacheva, A. Chernov, A. Shaposhnikov, A. Prokopov, V. Berzhansky, *et al.*, Generation of spin waves by a train of fs-laser pulses: A novel approach for tuning magnon wavelength, Sci. Rep. **7,** 5668 (2017).

[20] I. A. Filatov, P. Gerevenkov, M. Wang, A. Rushforth, A. Kalashnikova, and N. Khokhlov, Spectrum evolution and chirping of laser-induced spin wave packets in thin iron films, Appl. Phys. Lett. **120,** 112404 (2022).

[21] P. Gerevenkov, I. A. Filatov, A. Kalashnikova, and N. Khokhlov, Unidirectional propagation of spin waves excited by femtosecond laser pulses in a planar waveguide, Phys. Rev. Appl. **19,** 024062 (2023).

[22] D. Krichevsky, N. Gusev, D. Ignatyeva, A. Prisyazhnyuk, E. Y. Semuk, S. Polulyakh, V. Berzhansky, A. Zvezdin, and V. Belotelov, Unconventional spin dynamics in the non-collinear phase of a ferrimagnet, Phys. Rev. B **108,** 174442 (2023).

[23] D. O. Ignatyeva, P. O. Kapralov, K. H. Prabhakara, H. Yoshikawa, A. Tsukamoto, and V. I. Belotelov, Magnetization switching in the gdfeco films with in-plane anisotropy via femtosecond laser pulses, Molecules **26,** 6406 (2021).

[24] D. Bossini, V. I. Belotelov, A. K. Zvezdin, A. N. Kalish, and A. V. Kimel, Magnetoplasmonics and femtosecond optomagnetism at the nanoscale, ACS Photonics **3,** 1385 (2016).

[25] N. Maccaferri, Coupling phenomena and collective effects in resonant meta-atoms supporting both plasmonic and (opto-) magnetic functionalities: An overview on properties and applications, JOSA B **36,** E112 (2019).

[26] A. Dutta, A. V. Kildishev, V. M. Shalaev, A. Boltasseva, and E. E. Marinero, Surface-plasmon opto-magnetic field enhancement for all-optical magnetization switching, Opt. Mater. Express **7,** 4316 (2017).

[27] P. E. Zimnyakova, D. O. Ignatyeva, A. N. Kalish, X. Han, and V. I. Belotelov, Plasmonic dichroism and all-optical magnetization switching in nanophotonic structures with GdFeCo, Opt. Lett. **47,** 6049 (2022).

[28] D. Ignatyeva, C. Davies, D. Sylgacheva, A. Tsukamoto, H. Yoshikawa, P. Kapralov, A. Kirilyuk, V. Belotelov, and A. Kimel, Plasmonic layer-selective all-optical switching of magnetization with nanometer resolution, Nat. Commun. **10,** 4786 (2019).

[29] X. Yang, Y. Mou, R. Zapata, B. Reynier, B. Gallas, and M. Mivelle, An inverse faraday effect generated by linearly polarized light through a plasmonic nano-antenna, Nanophotonics **12,** 687 (2023).

[30] J. Qin, S. Xia, W. Yang, H. Wang, W. Yan, Y. Yang, Z. Wei, W. Liu, Y. Luo, L. Deng, *et al.*, Nanophotonic devices based on magneto-optical materials: Recent developments and applications, Nanophotonics **11,** 2639 (2022).

[31] D. O. Ignatyeva, D. M. Krichevsky, V. I. Belotelov, F. Royer, S. Dash, and M. Levy, All-dielectric magneto-photonic metasurfaces, J. Appl. Phys. **132,** 100902 (2022).

[32] A. I. Chernov, M. A. Kozhaev, D. O. Ignatyeva, E. N. Beginin, A. V. Sadovnikov, A. A. Voronov, D. Karki, M. Levy, and V. I. Belotelov, All-dielectric nanophotonics enables tunable excitation of the exchange spin waves, Nano. Lett. **20,** 5259 (2020).

[33] D. A. Sylgacheva, N. E. Khokhlov, P. I. Gerevenkov, I. A. Filatov, M. A. Kozhaev, I. V. Savochkin, A. N. Kalish, A. M. Kalashnikova, and V. I. Belotelov, Spatially selective excitation of spin dynamics in magneto-photonic crystals by spectrally tunable ultrashort laser pulses, Nanophotonics **11,** 3169 (2022).

[34] D. Krichevsky, D. Ignatyeva, V. Ozerov, and V. Belotelov, Selective and tunable excitation of standing spin waves in a magnetic dielectric film by optical guided modes, Phys. Rev. Appl. **15,** 034085 (2021).

[35] D. M. Krichevsky, V. A. Ozerov, A. V. Bel'kova, D. A. Sylgacheva, A. N. Kalish, S. A. Evstigneeva, A. S. Pakhomov, T. V. Mikhailova, S. D. Lyashko, A. L. Kudryashov, E. Y. Semuk, A. I. Chernov, V. N. Berzhansky, and V. I. Belotelov, Spatially inhomogeneous inverse faraday effect provides tunable nonthermal excitation of exchange dominated spin waves, Nanophotonics **13,** 299 (2024).

[36] E. R. Edwards, M. Buchmeier, V. E. Demidov, and S. O. Demokritov, Magnetostatic spin-wave modes of an in-plane magnetized garnet-film disk, J. Appl. Phys. **113,** 103901 (2013).

[37] G. Kakazei, P. Wigen, K. Y. Guslienko, V. Novosad, A. Slavin, V. Golub, N. Lesnik, and Y. Otani, Spin-wave spectra of perpendicularly magnetized circular submicron dot arrays, Appl. Phys. Lett. **85,** 443 (2004).

[38] S. Polulyakh, V. Berzhanskii, E. Semuk, V. Belotelov, P. Vetoshko, V. Popov, A. Shaposhnikov, A. Shumilov, and A.

Chernov, Ferromagnetic resonance and elastic vibrations in epitaxial yttrium iron garnet films, J. Exp. Theor. Phys. **132,** 257 (2021).

[39] Y. Li, V. V. Naletov, O. Klein, J. L. Prieto, M. Muñoz, V. Cros, P. Bortolotti, A. Anane, C. Serpico, and G. De Loubens, Nutation spectroscopy of a nanomagnet driven into deeply nonlinear ferromagnetic resonance, Phys. Rev. X **9,** 041036 (2019).

[40] O. Dobrovolskiy, S. Bunyaev, N. Vovk, D. Navas, P. Gruszecki, M. Krawczyk, R. Sachser, M. Huth, A. Chumak, K. Guslienko, and G. Kakazei, Spin-wave spectroscopy of individual ferromagnetic nanodisks, Nanoscale **12,** 21207 (2020).

[41] M. Deb, E. Popova, M. Hehn, N. Keller, S. Petit-Watelot, M. Bargheer, S. Mangin, and G. Malinowski, Femtosecond laser-excitation-driven high frequency standing spin waves in nanoscale dielectric thin films of iron garnets, Phys. Rev. Lett. **123,** 027202 (2019).

[42] M. Deb, E. Popova, H.-Y. Jaffrès, N. Keller, and M. Bargheer, Controlling high-frequency spin-wave dynamics using double-pulse laser excitation, Phys. Rev. Appl. **18,** 044001 (2022).

[43] M. Moharam, E. B. Grann, D. A. Pommet, and T. Gaylord, Formulation for stable and efficient implementation of the rigorous coupled-wave analysis of binary gratings, JOSA A **12,** 1068 (1995).

[44] L. Li, Fourier modal method for crossed anisotropic gratings with arbitrary permittivity and permeability tensors, J. Opt. A: Pure Appl. Opt. **5,** 345 (2003).

[45] D. O. Ignatyeva, D. Karki, A. A. Voronov, M. A. Kozhaev, D. M. Krichevsky, A. I. Chernov, M. Levy, and V. I. Belotelov, All-dielectric magnetic metasurface for advanced light control in dual polarizations combined with high-q resonances, Nat. Commun. **11,** 5487 (2020).

[46] A. Vansteenkiste, J. Leliaert, M. Dvornik, M. Helsen, F. Garcia-Sanchez, and B. Van Waeyenberge, The design and verification of mumax3, AIP Adv. **4,** 107133 (2014).

[47] L. Körber, G. Quasebarth, A. Otto, and A. Kákay, Finite-element dynamic-matrix approach for spin-wave dispersions in magnonic waveguides with arbitrary cross section, AIP Adv. **11,** 095006 (2021).

[48] P. E. Zimnyakova, D. O. Ignatyeva, D. Karki, A. A. Voronov, A. N. Shaposhnikov, V. N. Berzhansky, M. Levy, and V. I. Belotelov, Two-dimensional array of iron-garnet nanocylinders supporting localized and lattice modes for the broadband boosted magneto-optics, Nanophotonics **11,** 119 (2021).

[49] J. Park, P. Eames, D. Engebretson, J. Berezovsky, and P. Crowell, Spatially resolved dynamics of localized spin-wave modes in ferromagnetic wires, Phys. Rev. Lett. **89,** 277201 (2002).

[50] A. Barman, V. Kruglyak, R. Hicken, J. Rowe, A. Kundro-taite, J. Scott, and M. Rahman, Imaging the dephasing of spin wave modes in a square thin film magnetic element, Phys. Rev. B **69,** 174426 (2004).

[51] A. Osada, R. Hisatomi, A. Noguchi, Y. Tabuchi, R. Yamazaki, K. Usami, M. Sadgrove, R. Yalla, M. Nomura, and Y. Nakamura, Cavity optomagnonics with spin-orbit coupled photons, Phys. Rev. Lett. **116,** 223601 (2016).

[52] J. Graf, H. Pfeifer, F. Marquardt, and S. V. Kusminskiy, Cavity optomagnonics with magnetic textures: Coupling a magnetic vortex to light, Phys. Rev. B **98,** 241406 (2018).

Correction: During the proof process, the second affiliation was erroneously duplicated as the seventh affiliation. The seventh affiliation has been removed and the affiliation indicators for the last author have been fixed.